Influence of the Amazon River on the Nd isotope composition of deep water in the western equatorial Atlantic during the Oligocene–Miocene transition

Earth and Planetary Science Letters 454 (2016) 132–141

Contents lists available at ScienceDirect

Earth and Planetary Science Letters

www.elsevier.com/locate/epsl

Influence of the Amazon River on the Nd isotope composition of deep water in the western equatorial Atlantic during the Oligocene–Miocene transition

Joseph A. Stewart [a,b,*], Marcus Gutjahr [c], Rachael H. James [a], Pallavi Anand [d], Paul A. Wilson [a]

[a] National Oceanography Centre Southampton, University of Southampton, European Way, Southampton, SO14 3ZH, UK
[b] National Institute of Standards and Technology, Hollings Marine Laboratory, 331 Fort Johnson Rd, Charleston, SC, 29412, USA
[c] GEOMAR Helmholtz Centre for Ocean Research Kiel, Wischhofstraße 1-3, D-24148 Kiel, Germany
[d] School of Environment, Earth and Ecosystem Sciences, Walton Hall, The Open University, Milton Keynes, MK7 6AA, UK

ARTICLE INFO

Article history:
Received 26 May 2016
Received in revised form 25 August 2016
Accepted 26 August 2016
Available online xxxx
Editor: D. Vance

Keywords:
neodymium isotopes
fish teeth
foraminifera
Amazon
Oligocene–Miocene
ODP Site 926

ABSTRACT

Dissolved and particulate neodymium (Nd) are mainly supplied to the oceans via rivers, dust, and release from marine sediments along continental margins. This process, together with the short oceanic residence time of Nd, gives rise to pronounced spatial gradients in oceanic $^{143}Nd/^{144}Nd$ ratios (ε_{Nd}). However, we do not yet have a good understanding of the extent to which the influence of riverine point-source Nd supply can be distinguished from changes in mixing between different water masses in the marine geological record. This gap in knowledge is important to fill because there is growing awareness that major global climate transitions may be associated not only with changes in large-scale ocean water mass mixing, but also with important changes in continental hydroclimate and weathering. Here we present ε_{Nd} data for fossilised fish teeth, planktonic foraminifera, and the Fe–Mn oxyhydroxide and detrital fractions of sediments recovered from Ocean Drilling Project (ODP) Site 926 on Ceara Rise, situated approximately 800 km from the mouth of the River Amazon. Our records span the Mi-1 glaciation event during the Oligocene–Miocene transition (OMT; ~23 Ma). We compare our ε_{Nd} records with data for ambient deep Atlantic northern and southern component waters to assess the influence of particulate input from the Amazon River on Nd in ancient deep waters at this site. ε_{Nd} values for all of our fish teeth, foraminifera, and Fe–Mn oxyhydroxide samples are extremely unradiogenic ($\varepsilon_{Nd} \approx -15$); much lower than the ε_{Nd} for deep waters of modern or Oligocene–Miocene age from the North Atlantic ($\varepsilon_{Nd} \approx -10$) and South Atlantic ($\varepsilon_{Nd} \approx -8$). This finding suggests that partial dissolution of detrital particulate material from the Amazon ($\varepsilon_{Nd} \approx -18$) strongly influences the ε_{Nd} values of deep waters at Ceara Rise across the OMT. We conclude that terrestrially derived inputs of Nd can affect ε_{Nd} values of deep water many hundreds of kilometres from source. Our results both underscore the need for care in reconstructing changes in large-scale oceanic water-mass mixing using sites proximal to major rivers, and highlight the potential of these marine archives for tracing changes in continental hydroclimate and weathering.

1. Introduction

The weathering and transport of continental rock substrate is a major source of dissolved neodymium to the oceans (Goldstein and Jacobsen, 1987). The neodymium isotopic composition ($\varepsilon_{Nd} = [(^{143}Nd_{sample}/^{144}Nd_{sample})/(^{143}Nd_{CHUR}/^{144}Nd_{CHUR}) - 1] \times 10^4$; where CHUR is the chondritic uniform reservoir) of continental rocks varies according to both the Sm/Nd ratio and age of the rock, such that ancient continental crust exhibits very low (unradiogenic) ε_{Nd} values (down to −40), whereas younger volcanic sequences generally have much higher (radiogenic) values (up to +12; Goldstein and Hemming, 2003). Because neodymium has a residence time on the order of the mixing time of the ocean (500 to 2000 yr; Piepgras and Wasserburg, 1987; Tachikawa et al., 2003), deep waters formed in the North Atlantic, which is surrounded by Proterozoic and Archean rocks, are charac-

* Corresponding author at: National Institute of Standards and Technology, Hollings Marine Laboratory, 331 Fort Johnson Rd, Charleston, SC, 29412, USA.
E-mail address: Joseph.Stewart@noaa.gov (J.A. Stewart).

http://dx.doi.org/10.1016/j.epsl.2016.08.037

terised by low ε_{Nd} (−13.5; Piepgras and Wasserburg, 1987; Lacan and Jeandel, 2005a). On the other hand, deep water masses formed in the Southern Ocean have higher ε_{Nd} (between −7 and −9; Piepgras and Wasserburg, 1987; Jeandel, 1993; Stichel et al., 2012) due to the contribution of young mantle-derived material surrounding the Pacific Ocean that mixes with Atlantic waters in this region. Records of seawater ε_{Nd} values recorded in marine sediments have therefore been widely used to identify the source of the overlying water masses (e.g. Scher and Martin, 2004; Piotrowski et al., 2005; Bohm et al., 2015; Lang et al., 2016).

In addition to the influence of riverine solute inputs, the isotopic composition of dissolved Nd in seawater can be modified by exchange of Nd in river-born particulate material with seawater via "boundary exchange" on continental margins (Jeandel et al., 2007; Pearce et al., 2013) and also in certain deep sea settings (Lacan and Jeandel, 2005b; Carter et al., 2012; Wilson et al., 2012; Abbott et al., 2015b). Various modelling studies even suggest that release of Nd from continental margins is by far the dominant source of Nd to the oceans (contributing as much as 90%; Arsouze et al., 2009; Rempfer et al., 2011). Dissolved deep water ε_{Nd} at these continental margin locations is likely a function of three variables: (i) the magnitude of the Nd flux from sediment pore fluids, (ii) the difference between the ε_{Nd} value of the overlying water and the pore fluid, and (iii) the exposure time to this benthic flux of Nd (Abbott et al., 2015a).

The Amazon River is the world's largest river and each year carries 5×10^8 tons of suspended sediment (Gibbs, 1967) that is relatively enriched in Nd (~40 ppm; McDaniel et al., 1997) compared to seawater (typically <10 ppb; Piepgras and Wasserburg, 1987). These Nd-rich Amazon sediments have been shown to influence the dissolved ε_{Nd} of near-shore seawater (e.g. the mid-salinity zone of the Amazon Estuary; Rousseau et al., 2015), and have also been suggested to affect deep water ε_{Nd} as far afield as the Caribbean Sea (Osborne et al., 2014). An improved understanding of the extent to which river-born particulate material can influence deep water ε_{Nd} is, therefore, critical to our understanding of Nd cycling in the oceans (Stichel et al., 2012; Kraft et al., 2013; Pearce et al., 2013). This is particularly true for major climate transitions when rock weathering and the flux of riverine particulate material may vary (West et al., 2005), centres of precipitation can shift altering river drainage patterns (Wang et al., 2004), and ocean circulation can change the exposure time of water masses to benthic sources of Nd (Abbott et al., 2015a). Records of past seawater and associated sediment ε_{Nd} in relative proximity to major riverine sources of Nd such as the Amazon River are therefore vital to understanding Nd exchange between particulate and dissolved phases in continental margin settings.

1.1. Archives of seawater ε_{Nd}

Fossilised fish teeth recovered from deep sea sediment cores are an ideal substrate for reconstructing past changes in ε_{Nd} values of ancient bottom waters. Fish teeth are found throughout the world's oceans and incorporate the majority of their Nd post-mortem (>100 ppm Nd), during early diagenetic recrystallization of the biogenic apatite at the sediment-seawater interface. They are therefore resistant to late diagenetic overprinting (Martin and Scher, 2004). Analysis of Nd associated with authigenic Fe–Mn oxyhydroxides in marine sediments can also be used to extract bottom water Nd isotope compositions (Piotrowski et al., 2005), although care must be taken during sample processing (Elmore et al., 2011).

The only method by which ε_{Nd} values of surface waters have been successfully reconstructed to date is through the analysis of reductively cleaned planktonic foraminifera (Vance and Burton, 1999). However, because diagenetic ferromanganese coatings formed on the seafloor and in pore waters are extremely enriched in Nd (200 ppm) compared with biogenic calcite (0.1 ppm), these coatings must be effectively removed (Pomiès et al., 2002). ε_{Nd} records of cleaned planktonic foraminifera that have elevated Nd/Ca are likely compromised by incomplete removal (<98%) of ferromanganese coatings or reabsorption of Nd released during the cleaning process. For this reason, even cleaned foraminifera often exhibit ε_{Nd} values similar to bottom waters (Roberts et al., 2012; Tachikawa et al., 2014).

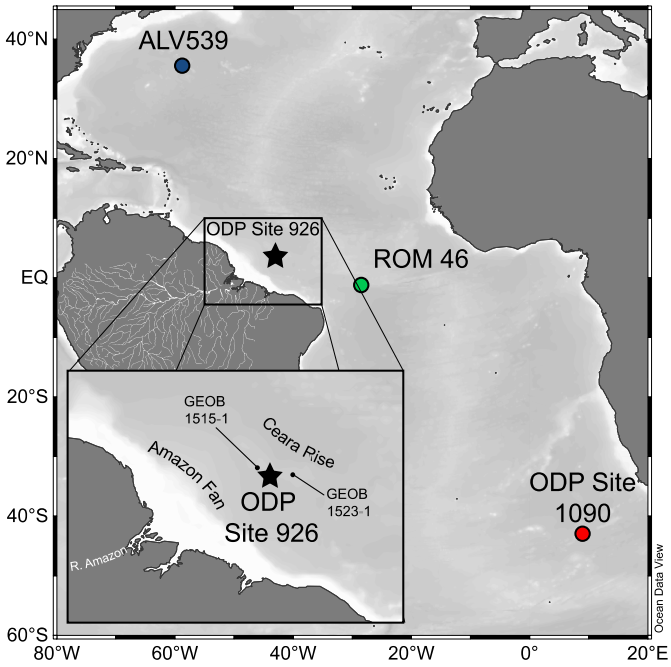

Fig. 1. Location of ODP Leg 154 Site 926B Ceara Rise in relation to other deep water ε_{Nd} records across the Oligocene–Miocene transition discussed in this study. Fe–Mn crust ALV539, 2,665 m water depth (O'Nions et al., 1998), Fe–Mn crust ROM46, 3,350 m water depth (Frank et al., 2003), Fish tooth record from ODP Site 1090, 3,700 m water depth (Scher and Martin, 2008). Colours correspond to line/marker colours in Fig. 2. Inset shows location of ODP Site 926B in relation to the Amazon River mouth and piston core sites on Ceara Rise, GEOB 1515-1 (3,129 m water depth) and GEOB 1523-1 (3,292 m water depth) used in the study by Lippold et al. (2016).

1.2. Scope of this study

Here we assess evidence for changes in continental inputs from the Amazon River during the Oligocene–Miocene transition (OMT), through analysis of ε_{Nd} in fish teeth, planktonic foraminifera, and the Fe–Mn oxyhydroxide and detrital fractions of sediments recovered from ODP Site 926 (Fig. 1). The OMT is marked by a positive excursion (>1‰) in benthic foraminiferal $\delta^{18}O$ at 23 Ma (Fig. 2) that represents cooler deep-water temperatures and increased Antarctic ice volume associated with the so-called Mi-1 glaciation event (Pälike et al., 2006; Liebrand et al., 2011, 2016). We use our ε_{Nd} data to assess the contribution of the Amazon as a source of Nd to the regional Equatorial Atlantic water mass signal at this site during this interval of climatic variability, and discuss the implications of these data for interpretation of ε_{Nd} records in terms of water mass mixing.

2. Materials and methods

2.1. Geological setting and core chronology

Samples spanning the OMT were selected from sediment cores recovered from ODP Leg 154, Site 926, Hole B (3°43.148′N, 42°54.507′W, ~3600 m water depth; Leg 154 Shipboard Scientific Party, 1995), situated approximately 800 km to the northeast

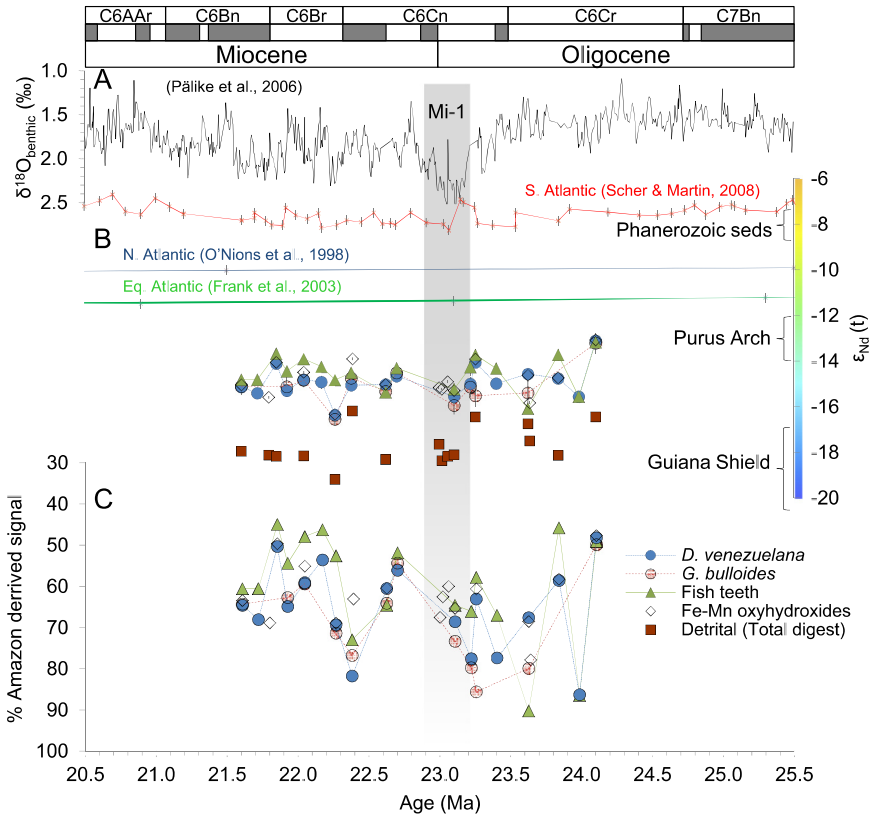

Fig. 2. ε_{Nd} records across the Oligocene–Miocene transition at ODP Site 926. **A.** Benthic oxygen isotope record for this site (Pälike et al., 2006), **B.** ε_{Nd} values for fossilised fish teeth (green triangles), planktonic foraminifera *D. venezuelana* (blue circles) and *G. bulloides* (red circles), Fe/Mn oxyhydroxides (black diamonds), and the detrital fraction (squares). Deep water ε_{Nd} values for the South Atlantic (Scher and Martin, 2008), Equatorial Atlantic (Frank et al., 2003), and North Atlantic (O'Nions et al., 1998) at the OMT are also shown for comparison. Colour scale corresponds to that used in Fig. 3 showing potential Amazon basin source rock ε_{Nd} ranges for Guiana Shield, Purus Arch and Phanerozoic sediments (Allègre et al., 1996). **C.** Estimated percentage of ε_{Nd} seawater signal at Ceara Rise coming from Amazon sources relative to northern component water during the OMT. Error bars represent the 2 standard error of each measurement. Magnetostratigraphic correlation from ODP Site 1090 in the South Atlantic (Billups et al., 2002; Channell et al., 2003). (For interpretation of the references to colour in this figure legend, the reader is referred to the web version of this article.)

of the mouth of the River Amazon (Fig. 1). The geographic position and water-depth of Site 926 have not changed significantly since the Oligocene. Although there is no magnetostratigraphic age control available for ODP Leg 154 cores, a high quality orbital chronology is available for the Oligocene–Miocene sequence at ODP Site 926 (Pälike et al., 2006) and can be correlated to ODP Site 1090 on the Agulhas Ridge (Liebrand et al., 2011) where a high quality magnetostratigraphy is available (Fig. 2; Channell et al., 2003). We apply the age model of Pälike et al. (2006).

2.2. Sample preparation

Sediment samples were dried in an oven at 50 °C, then gently disaggregated in deionised water using a shaker table and washed over a 63 μm sieve. Tests (~1 mg) of the planktonic foraminifer *Dentoglobigerina venezuelana* were picked from the 355–400 μm size fraction for trace element analysis (see Supplementary Information) following the morphotype description of Stewart et al. (2012). Larger samples of *D. venezuelana* (~25 mg) and a second species, *Globigerina bulloides* (~5 mg), were picked for Nd isotope analysis from the >355 μm size fraction. Additionally, fossilised fish teeth (and one fish bone sample) were taken for ε_{Nd} analysis. These samples consisted of an average of three individual teeth.

2.2.1. Detrital and authigenic Fe–Mn oxyhydroxide extraction

Dried and ground bulk sediment (~420–610 mg) was transferred into centrifuge tubes for processing. After an initial wash in MQ water and centrifuging, 15 ml of a reductive cocktail containing 0.05 M hydroxylamine hydrochloride, 15% acetic acid, and 0.01 M buffered EDTA was added following methods of Blaser et al. (2016), with reductive cocktail concentrations as used in Gutjahr et al. (2007). Samples were centrifuged and the supernatant was removed for purification of Nd from the Fe–Mn oxyhydroxide fraction. Another 25 ml of the reductive leaching solution was added to remove any remaining Fe–Mn oxyhydroxides (Gutjahr et al., 2007) in order to target the pure terrigenous signal without residual authigenic Nd contributions. After shaking for 24 h, the supernatant was discarded following centrifuging and the sample was dried. Approximately 50 mg of the dried re-homogenised residue was first treated with concentrated HNO_3 and 30% H_2O_2 for effective oxidation of organics. Dried samples were subsequently treated with aqua regia prior to pressure digestion in steel bombs (190 °C over three days) in a mixture of concentrated HNO_3 and HF. Dried digested samples were treated three times with concentrated HNO_3 before conversion to chloride with HCl and column purification using procedures outlined in Section 2.2.3.

2.2.2. Foraminifera and fish tooth cleaning procedure

All foraminifera and fish teeth samples were subject to cleaning prior to analysis using established methods (Rosenthal et al., 1999). Briefly, adhering clay particles were removed through repeated ultrasonication and rinsing with MQ water and methanol. Samples were then cleaned to remove ferromanganese oxide coatings and organic matter, and finally leached in weak acid to remove any re-adsorbed ions. Foraminiferal calcite and fish teeth samples for isotopic analysis were dissolved in 0.075 M and 0.15 M HNO_3 respectively.

Table 1
ε_{Nd} measurements of detrital sediments and Fe/Mn oxyhydroxides from the Oligocene–Miocene transition of ODP Site 926. Ages are calculated using the age model of Pälike et al. (2006). $\varepsilon_{Nd}(0)$ denotes measured ε_{Nd} values, and $\varepsilon_{Nd}(t)$ values have been adjusted for ingrowth of ^{143}Nd since the Oligocene (assumption: initial $^{147}Sm/^{144}Nd$ ratio 0.1412 for detrital and Fe–Mn oxyhydroxide samples).

ODP Sample Identification Site, Hole, Core, Section, Half, Int.		Depth (mbsf)	Age (Ma)	Detrital (Total digest)			2SE	Fe–Mn oxyhydroxides			2SE
				$^{143}Nd/^{144}Nd$ (normalised)	$\varepsilon_{Nd}(0)$	$\varepsilon_{Nd}(t)$		$^{143}Nd/^{144}Nd$ (normalised)	$\varepsilon_{Nd}(0)$	$\varepsilon_{Nd}(t)$	
926 B 46 4 W	40–50	427.8	**21.61**	0.511710	−18.10	**−17.95**	0.06	0.511859	−15.20	**−15.04**	0.05
926 B 46 6 W	70–80	431.1	**21.72**								
926 B 47 1 W	65–67	433.1	**21.80**	0.511701	−18.27	**−18.12**	0.05	0.511831	−15.74	**−15.59**	0.06
926 B 47 2 W	70–80	434.7	**21.85**	0.511698	−18.33	**−18.17**	0.05	0.511909	−14.21	**−14.06**	0.08
926 B 47 4 W	10–20	437.1	**21.93**								
926 B 47 6 W	42–50	440.4	**22.05**	0.511700	−18.30	**−18.15**	0.06	0.511887	−14.64	**−14.49**	0.06
926 B 48 2 W	72–80	444.4	**22.17**								
926 B 48 4 W	52–60	447.2	**22.27**	0.511647	−19.34	**−19.18**	0.05	0.511793	−16.49	**−16.33**	0.05
926 B 48 6 W	91–100	450.6	**22.38**								
926 B 48 6 W	132–134	450.9	**22.39**	0.511800	−16.34	**−16.19**	0.05	0.511917	−14.06	**−13.90**	0.06
926 B 49 4 W	109–120	457.3	**22.62**	0.511691	−18.47	**−18.31**	0.05	0.511860	−15.18	**−15.02**	0.04
926 B 49 6 W	5–15	459.3	**22.70**								
926 B 50 4 W	102–105	466.9	**23.00**	0.511725	−17.81	**−17.64**	0.04	0.511852	−15.32	**−15.16**	0.05
926 B 50 5 W	5.5–7.5	467.5	**23.02**	0.511688	−18.52	**−18.36**	0.05	0.511849	−15.39	**−15.23**	0.05
926 B 50 5 W	111–114	468.5	**23.06**	0.511698	−18.34	**−18.18**	0.05	0.511866	−15.07	**−14.90**	0.04
926 B 50 6 W	82–92	469.8	**23.11**	0.511702	−18.27	**−18.10**	0.04	0.511846	−15.45	**−15.29**	0.05
926 B 51 2 W	35–45	472.9	**23.22**								
926 B 51 2 W	128–133	473.8	**23.26**	0.511786	−16.61	**−16.45**	0.05	0.511917	−14.07	**−13.91**	0.06
926 B 51 5 W	53–60	477.6	**23.40**								
926 B 52 1 W	94–104	481.5	**23.63**	0.511771	−16.91	**−16.75**	0.06	0.511880	−14.79	**−14.62**	0.06
926 B 52 1 W	141–143	481.9	**23.64**	0.511733	−17.66	**−17.49**	0.05	0.511818	−16.00	**−15.83**	0.05
926 B 52 5 W	29–38	486.8	**23.84**	0.511700	−18.29	**−18.12**	0.05	0.511874	−14.90	**−14.73**	0.05
926 B 53 1 W	35–44	490.6	**23.99**								
926 B 53 3 W	105–114	494.3	**24.10**	0.511786	−16.62	**−16.44**	0.04	0.511959	−13.24	**−13.07**	0.05

2.2.3. Separation of Nd from the sample matrix

Nd was separated from the sample matrix using a two-stage chromatography procedure. Sample solutions were dried down on a hotplate and then re-dissolved in 0.2 M HCl. This solution was then loaded onto a Teflon column containing 2.4 ml of Bio-Rad™ AG50W-X12 cation exchange resin. Matrix elements were removed by eluting with 4 M HCl. Rare earth elements were then collected in 6 M HCl. The recovered rare earth fraction was dried down, re-dissolved in 0.18 M HCl, and loaded onto a second cation exchange column containing 0.6 ml of Eichron™ Ln spec resin of particle size 50 to 100 µm. Residual Sr and approximately 90% of the Ce were first eluted with 8 ml of 0.18 M HCl, and the Nd fraction was collected by addition of a further 7 ml of 0.18 M HCl. The total procedural blank from the columns was 13 pg of Nd, which is typically $\ll$1% of the sample size.

2.3. Analytical techniques

Details and results of analysis of Nd/Ca and Mn/Ca in foraminiferal calcite are shown in the Supplementary Information. The Nd isotopic composition of the fish teeth and foraminifera was determined by multicollector inductively coupled plasma mass spectrometry (MC-ICP-MS; ThermoFisher Neptune) at the University of Southampton, and the Nd isotopic composition of the sediment leaches and digests was carried out at GEOMAR in Kiel (MC-ICP-MS; ThermoFisher Neptune Plus), using the method of Vance and Thirwall (2002). Measured $^{143}Nd/^{144}Nd$ ratios were corrected to a $^{146}Nd/^{144}Nd$ ratio of 0.7219 to remove mass bias effects (Wombacher and Rehkämper, 2003). The external reproducibility of our Nd isotope measurements, for Nd solutions of 25 to 50 ppb is better than $\pm$0.16 ($n = 37$) and $\pm$0.11 ($n = 19$) ε units (2σ) in Southampton and Kiel, respectively. Corrected data were normalised by adjusting the average $^{143}Nd/^{144}Nd$ ratio of the JNdi-1 Nd isotope standard measured during that analytical session to the accepted value of 0.512115 (Tanaka et al., 2000). $^{143}Nd/^{144}Nd$ ratios ($\varepsilon_{Nd(0)}$) were corrected for post-depositional ingrowth of ^{143}Nd from ^{147}Sm ($\varepsilon_{Nd(t)}$) using an initial $^{147}Sm/^{144}Nd$ ratio of 0.1286 for fish teeth (Thomas et al., 2003) and 0.1412 for foraminifera, detrital and Fe–Mn oxyhydroxide samples (Vance et al., 2004). This adjustment is small for our samples (lowering ε_{Nd} by $<$0.17 units). All subsequent discussion refers to the adjusted $\varepsilon_{Nd(t)}$ values.

3. Results

In Fig. 2 we compare our records of ε_{Nd} in the detrital fraction, Fe–Mn oxyhydroxides (Table 1), fish teeth, and foraminifera (*D. venezuelana*, and *G. bulloides*; Table 2) from ODP Site 926 with the benthic foraminiferal oxygen isotope record from the same site (Fig. 2A; Pälike et al., 2006). We further compare these ε_{Nd} measurements to records of representative contemporaneous deep water ε_{Nd} (Fig. 1; Fig. 2B) from the North (Fe–Mn crust ALV539; O'Nions et al., 1998), South (fish teeth from ODP Site 1090; Scher and Martin, 2008), and Equatorial Atlantic Ocean (Fe–Mn crust ROM46; Frank et al., 2003). With the exception of the North Atlantic Fe–Mn crust site ALV539 (depth 2.7 km) the water depths (and palaeodepths) of all of these sites are similar to that of Ceara Rise (Fig. 1). Despite its slightly shallower depth, we assume that the ε_{Nd} of seawater at Site ALV539 is typical of northern sourced deep water to Ceara Rise.

Most of our data for the detrital fraction from the OMT at Ceara Rise show distinctly unradiogenic ε_{Nd} values with a baseline of around -18 ε units. Four samples show slightly more radiogenic values (around -16.5 ε units) at 22.4, 23.3, 23.6, and 24.1 Ma but the occurrence of these data points shows no clear correspondence to structure in the benthic foraminiferal oxygen isotope stratigraphy from the same site.

ε_{Nd} values for fish teeth are, on average, -14.5 and all data points are lower than -13.0 ε units. The foraminiferal ε_{Nd} records for *D. venezuelana* and *G. bulloides* are generally within analytical uncertainty of one another and vary between -16.5 and -13.2 ε units. Compositions of the Fe–Mn oxyhydroxide fraction are within 0.26 ε units of the foraminiferal ε_{Nd} values. Furthermore, the pattern of change seen in the Fe–Mn oxyhydroxide and foraminiferal ε_{Nd} records is remarkably similar to that of the fish teeth record. We therefore find no discernible difference between the fish teeth,

Table 2
ε_{Nd} measurements of fossilised fish teeth and planktonic foraminifera (*D. venezuelana* and *G. bulloides*) from the Oligocene–Miocene transition of ODP Site 926. Ages are calculated using the age model of Pälike et al. (2006). $\varepsilon_{Nd}(0)$ denotes measured ε_{Nd} values, and $\varepsilon_{Nd}(t)$ values have been adjusted for ingrowth of ^{143}Nd since the Oligocene (assumption: initial $^{147}Sm/^{144}Nd$ ratio 0.1286 for fish teeth and 0.1412 for foraminifera samples).

ODP Sample Identification Site, Hole, Core, Section, Half, Int.		Depth (mbsf)	Age (Ma)	Fish teeth			2SE	*D. venezuelana*			2SE	*G. bulloides*			2SE
				$^{143}Nd/^{144}Nd$ (normalised)	$\varepsilon_{Nd}(0)$	$\varepsilon_{Nd}(t)$		$^{143}Nd/^{144}Nd$ (normalised)	$\varepsilon_{Nd}(0)$	$\varepsilon_{Nd}(t)$		$^{143}Nd/^{144}Nd$ (normalised)	$\varepsilon_{Nd}(0)$	$\varepsilon_{Nd}(t)$	
926 B 46 4 W	40–50	427.8	**21.61**	0.511869	−15.00	**−14.81**	0.19	0.511854	−15.28	**−15.13**	0.22	0.511856	−15.26	**−15.11**	0.39
926 B 46 6 W	70–80	431.1	**21.72**	0.511869	−15.00	**−14.81**	0.18	0.511840	−15.56	**−15.41**	0.20				
926 B 47 1 W	65–67	433.1	**21.80**												
926 B 47 2 W	70–80	434.7	**21.85**	0.511928	−13.86	**−13.67**	0.17	0.511907	−14.26	**−14.11**	0.21				
926 B 47 4 W	10–20	437.1	**21.93**	0.511888	−14.63	**−14.44**	0.19	0.511846	−15.45	**−15.30**	0.23	0.511855	−15.27	**−15.12**	0.46
926 B 47 6 W	42–50	440.4	**22.05**	0.511916	−14.09	**−13.90**	0.19	0.511871	−14.96	**−14.81**	0.20	0.511870	−14.99	**−14.83**	0.31
926 B 48 2 W	72–80	444.4	**22.17**	0.511898	−14.43	**−14.25**	0.18	0.511865	−15.07	**−14.92**	0.27				
926 B 48 4 W	52–60	447.2	**22.27**	0.511868	−15.02	**−14.83**	0.19	0.511791	−16.52	**−16.36**	0.17	0.511782	−16.70	**−16.55**	0.25
926 B 48 6 W	91–100	450.6	**22.38**	0.511884	−14.70	**−14.51**	0.18	0.511858	−15.21	**−15.06**	0.23	0.511874	−14.90	**−14.75**	0.24
926 B 48 6 W	132–134	450.9	**22.39**												
926 B 49 4 W	109–120	457.3	**22.62**	0.511841	−15.56	**−15.36**	0.18	0.511860	−15.18	**−15.03**	0.16	0.511844	−15.48	**−15.32**	0.27
926 B 49 6 W	5–15	459.3	**22.70**	0.511895	−14.50	**−14.31**	0.20	0.511878	−14.82	**−14.66**	0.20	0.511886	−14.67	**−14.51**	0.19
926 B 50 4 W	102–105	466.9	**23.00**												
926 B 50 5 W	5.5–7.5	467.5	**23.02**												
926 B 50 5 W	111–114	468.5	**23.06**												
926 B 50 6 W	82–92	469.8	**23.11**	0.511847	−15.43	**−15.23**	0.26	0.511832	−15.72	**−15.56**	0.20	0.511813	−16.10	**−15.94**	0.40
926 B 51 2 W	35–45	472.9	**23.22**	0.511897	−14.46	**−14.26**	0.36	0.511861	−15.16	**−15.00**	0.25	0.511854	−15.30	**−15.14**	0.43
926 B 51 2 W	128–133	473.8	**23.26**	0.511924	−13.92	**−13.72**	0.24	0.511909	−14.23	**−14.06**	0.22	0.511834	−15.68	**−15.52**	0.50
926 B 51 5 W	53–60	477.6	**23.40**	0.511894	−14.52	**−14.32**	0.20	0.511861	−15.15	**−14.99**	0.24				
926 B 52 1 W	94–104	481.5	**23.63**	0.511803	−16.29	**−16.09**	0.16	0.511883	−14.72	**−14.56**	0.18	0.511841	−15.55	**−15.39**	0.71
926 B 52 1 W	141–143	481.9	**23.64**												
926 B 52 5 W	29–38	486.8	**23.84**	0.511924	−13.92	**−13.72**	0.25	0.511873	−14.92	**−14.76**	0.21				
926 B 53 1 W	35–44	490.6	**23.99**	0.511830	−15.77	**−15.57**	0.19	0.511832	−15.72	**−15.56**	0.24				
926 B 53 3 W	105–114	494.3	**24.10**	0.511953	−13.37	**−13.16**	0.26	0.511958	−13.27	**−13.11**	0.21	0.511952	−13.38	**−13.21**	0.45

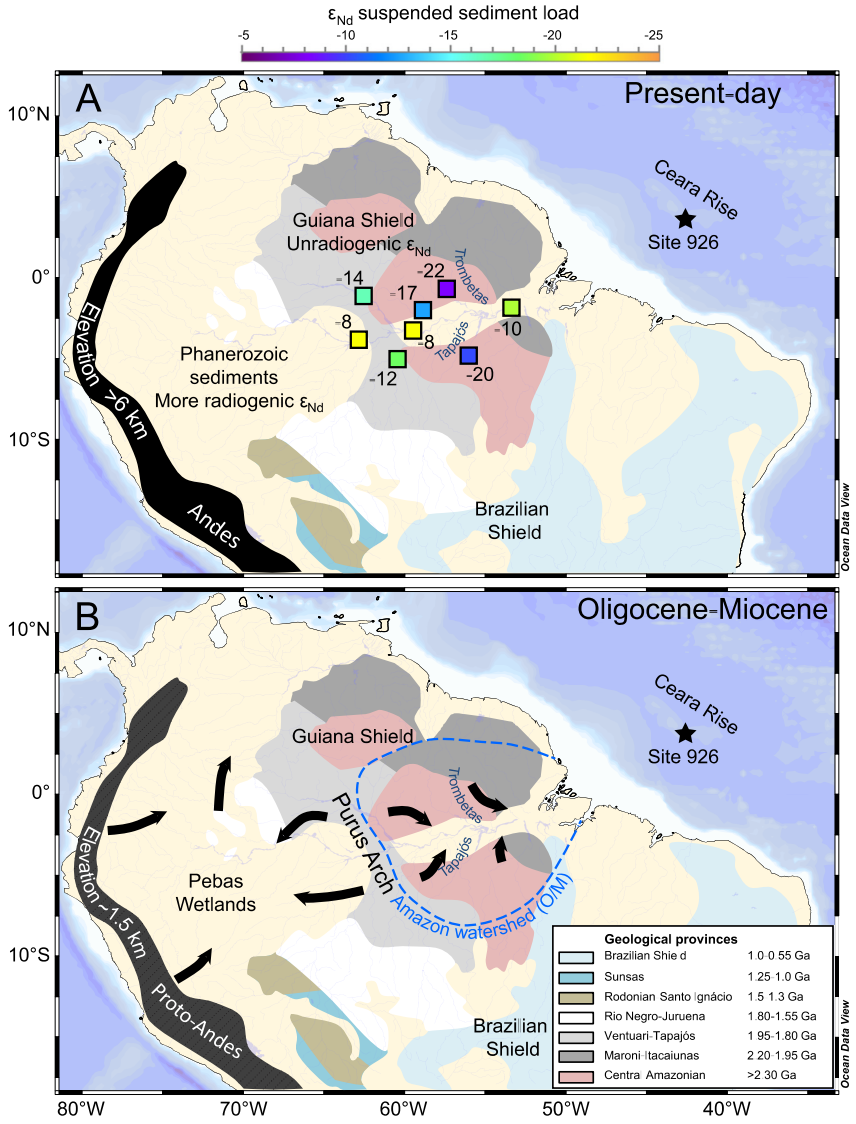

Fig. 3. Geology of the Amazon Basin. Star shows the position of ODP Site 926 on Ceara Rise. Panel A. Coloured squares (colour scale corresponds to that used in Fig. 2) show ε_{Nd} values of modern suspended sediments in Amazon tributaries (Allègre et al., 1996). Shaded regions show basement lithology. Panel B. Amazon drainage during the Oligocene–Miocene. Black arrows and blue dashed line show, respectively, the inferred drainage pattern and catchment area at this time (Figueiredo et al., 2009; Shephard et al., 2010). (For interpretation of the references to colour in this figure legend, the reader is referred to the web version of this article.)

foraminifera, and Fe–Mn oxyhydroxide ε_{Nd} records, even during the large oxygen isotope excursion corresponding to the Mi-1 glaciation event.

4. Discussion

To assess the potential influence of input of riverine particulate material from the Amazon to Ceara Rise, we first discuss the Nd isotope composition of the detrital fraction of the sediments. We then assess the impact of the Amazon on the Nd isotopic composition of seawater in the western equatorial Atlantic across the OMT by comparing Nd isotope compositions in the three different palaeo-seawater substrates.

4.1. Source of detrital sediments at Ceara Rise

The Nd isotopic composition of the detrital fraction of the sediments is used to assess the Nd isotopic signature of terrestrial material from the Amazon River reaching the Ceara Rise during the OMT. Sediment particles delivered to the modern Amazon Fan from the River Amazon and its tributaries exhibit a wide range of ε_{Nd} values today (from −8 to −22; Allègre et al., 1996), reflecting the variable age of the catchment bedrock (Fig. 3A). Unradiogenic ε_{Nd} values are observed in the eastern tributaries (Tapajós tributary $\varepsilon_{Nd} = -20$, Trombetas tributary $\varepsilon_{Nd} = -22$; Allègre et al., 1996), which drain ancient cratonic sequences of the Guiana Shield (>2.3 Ga). By contrast, the western tributaries draining younger Phanerozoic sedimentary rocks have more radiogenic sedimentary particulate loads ($\varepsilon_{Nd} \sim -8$). These eroded sediments from the east and west tributaries combine to give an intermediate ε_{Nd} value for the modern Amazon suspended sediment load output to the Atlantic Ocean, which has $\varepsilon_{Nd} = -10$ (Allègre et al., 1996; McDaniel et al., 1997; Rousseau et al., 2015). These large regional distinctions in ε_{Nd} composition between geological terranes mean that changes in drainage patterns have the potential to give rise to dramatic changes in the ε_{Nd} of riverine suspended sediments to the Atlantic Ocean.

The drainage of the Amazon during the Oligocene and Miocene is thought to have been very different from today because of the lower altitude of the Andes (Fig. 3B; Campbell et al., 2006; Figueiredo et al., 2009; Shephard et al., 2010). Stratigraphic records suggest that, prior to the middle-Miocene (Cunha et al., 1994;

Eiras et al., 1994), the Amazon Basin consisted of two catchments divided by the Purus Arch: the Eastern Amazon basin to the east and the Pebas Wetlands to the west (Figueiredo et al., 2009). Under this configuration, the outflow from the Amazon to the Atlantic would have originated almost exclusively from the Eastern Amazon Basin, which is underlain by the Guiana Shield and today yields very unradiogenic ε_{Nd} values for suspended loads, between −17 and −22 (Allègre et al., 1996). The low ε_{Nd} values recorded in the detrital fraction (−18 ε units) that we document at Site 926, together with colour, grain-size and rare earth element logs of sediments recovered from other ODP Leg 154 sites (Dobson et al., 2001), all suggest that the Guiana Shield was the dominant source of terrigenous sediment to Ceara Rise throughout our study interval.

Four samples in our data set show higher ε_{Nd} in the detrital fraction (up to −16.5) and are interpreted to reflect the incorporation of detrital material from more radiogenic terranes adjacent to the ancient Guiana Shield. One possible source of more radiogenic Nd is the westerly Purus Arch (Fig. 3B). Changes in Amazon vegetation cover (e.g. van der Hammen and Hooghiemstra, 2000) and distribution of precipitation have been linked to global climate (Wang et al., 2004), as centres of tropical precipitation are often shifted meridionally away from the hemisphere of maximum cooling (Arbuszewski et al., 2013). Nearly all detrital ε_{Nd} values are slightly higher (more radiogenic) before the Mi-1 event than they are afterwards, but there is no obvious relationship between our detrital ε_{Nd} record and the benthic $\delta^{18}O$ record across the OMT (Fig. 2A; Pälike et al., 2006), even during the Mi-1 glaciation. We therefore conclude that changes in the source of Amazonian terrigenous sediment to Site 926 during our study interval are not strongly modulated by processes coupled to changes in high latitude temperature and continental ice volume. On the other hand, our data indicate that measurement of detrital ε_{Nd} of more recent Ceara Rise sediments (e.g. McDaniel et al., 1997) could represent a powerful tool for determining the disputed timing of westward enlargement of the Amazon Basin to its modern configuration during the Miocene/Pliocene (Campbell et al., 2006; Figueiredo et al., 2009).

4.2. Nd in fish teeth and fossilised foraminifera at Ceara Rise

Of the data types presented here, those generated using fish teeth are commonly regarded as the most robust archive of changes in oceanic bottom water ε_{Nd} because most of the Nd contained in fish tooth fluorapatite is acquired during early diagenesis on the seafloor (Martin and Haley, 2000; Martin and Scher, 2004). In our study, ε_{Nd} data from planktonic foraminifera are strikingly similar to data from fish teeth and the authigenic Fe–Mn oxyhydroxide fraction, despite reductive cleaning that is expected to remove authigenic overgrowths from test calcite. While it is possible that the ε_{Nd} value of surface water was identical to the ε_{Nd} value of bottom water during the OMT, high Mn/Ca (>500 μmol/mol) and Nd/Ca (>1 μmol/mol) ratios measured in these foraminifera (see Supplementary Information) imply that the Nd in these samples more likely has an authigenic origin and is not representative of surface water (Pomiès et al., 2002; Tachikawa et al., 2014).

4.3. Sources of Nd to deep water at Ceara Rise

Fish teeth ε_{Nd} records from South Atlantic ODP Sites 689, Maud Rise (Scher and Martin, 2004) and 1090, Agulhas Ridge (Scher and Martin, 2006; Fig. 2B) suggest that, during the OMT, Atlantic deep waters originating in the Southern Ocean had ε_{Nd} values close to those of modern southern component water ($\varepsilon_{Nd} \sim -8$). Unradiogenic ε_{Nd} values typical of modern northern component deep water (−13.5; principally North Atlantic Deep Water; Piepgras and Wasserburg, 1987; Lacan and Jeandel, 2005a) only appear in the marine sedimentary record in the late Neogene, following closure of the Central American Seaway (Burton et al., 1997). The ε_{Nd} value of northern component deep water in the Miocene is estimated to have been much higher (∼−10; O'Nions et al., 1998; Scher and Martin, 2006) than its present day composition. Thus, simple mixing between northern and southern component deep waters cannot explain the low ε_{Nd} that we document in fish teeth, planktonic foraminifera, and the authigenic Fe–Mn fraction of sediments from Site 926 (∼−15 ε_{Nd} units; Fig. 2B). Rather, the deep waters must be affected by input of very unradiogenic Nd from a regional source, a clear candidate being the River Amazon.

Neodymium is exported from rivers to the oceans in three main phases, (i) dissolved Nd (Goldstein and Jacobsen, 1987), (ii) pre-formed oxides (Bayon et al., 2004), and (iii) Nd contained in detrital suspended particulate matter (Pearce et al., 2013). Various lines of evidence point to detrital particulate-bound supply as the major influence on deep water ε_{Nd} at Ceara Rise. First, dissolved Nd concentration in the modern Amazon Estuary is observed to increase in the mid-salinity zone and is accompanied by a shift in ε_{Nd} from riverine values (>−9) to values closer to the suspended load (<−10) (Rousseau et al., 2015). Therefore, Nd in the dissolved phase of Amazon river waters is extremely susceptible to alteration by Nd released from suspended particles during estuarine mixing. Second, if pre-formed Fe–Mn oxides were controlling the bottom water Nd isotope signature at Ceara Rise, this should be most clearly identifiable in isotopic differences between fish tooth- and Fe–Mn oxyhydroxide-derived ε_{Nd}. In such a scenario, the Fe–Mn oxyhydroxides would yield ε_{Nd} values similar to the detrital composition (cf. Bayon et al., 2004; Kraft et al., 2013). By contrast, the Nd incorporated into fish teeth is derived from bottom waters or pore fluids (Martin and Scher, 2004). Hence, our data indicate that pore fluid and bottom water ε_{Nd} at Ceara Rise differed from that of deep water in the central Atlantic (with $\varepsilon_{Nd} \sim -10$; O'Nions et al., 1998). The most likely reason for this is partial dissolution of Amazon particulate material within Ceara Rise pore fluids (Lacan and Jeandel, 2005a; Carter et al., 2012; Pearce et al., 2013; Abbott et al., 2015a). Once delivered to Ceara Rise, this particulate-bound Nd is transferred to the overlying deep waters through dissolution or desorption, thus shifting the deep water signal regionally towards less radiogenic ε_{Nd} values. Discovery of this signal at a site more than 800 km from the outflow source, in 3.6 km water depth, indicates that this process is not restricted to the continental shelves and can operate further offshore if particle fluxes are high.

To assess the percentage contribution of detrital Amazon-derived Nd to deep water ε_{Nd} at this site we compare fish tooth, foraminifera, and Fe–Mn oxyhydroxide data, with ε_{Nd} measurements of the corresponding detrital fraction and open ocean seawater. In this analysis, we used the detrital measurement closest to the sample depth of the fish tooth, foraminifera and leachate data where data from the same sample was not available (we note that our choice between detrital data from identical or adjacent samples for comparison to estimates of seawater ε_{Nd} has little impact on the main findings of this study). Assuming that the ε_{Nd} value of northern component water bathing Ceara Rise during the OMT was −10 (O'Nions et al., 1998), we calculate that the majority of the Nd in bottom waters at this site (average 64%) was derived from Amazon particulate material (Fig. 2C). Although we observe large amplitude variability in our down-core record (between 45% and 90%) that is likely related to variations in sediment sourcing from various Amazon tributaries (Fig. 3), there is no clear link between short-term increases/decreases in the estimated fraction of Amazon particulate-derived Nd on the ε_{Nd} signal of Ceara Rise bottom water and pronounced changes in high latitude cli-

mate inferred from benthic foraminiferal $\delta^{18}O$ (Fig. 2A; Pälike et al., 2006).

We note that ε_{Nd} values for deep water of similar age and water depth to our samples derived from a Fe–Mn crust (ROM46) recovered from the central Equatorial Atlantic Ocean are also relatively unradiogenic (−11.5; Fig. 2B), and also cannot therefore be explained by simple mixing between northern and southern component deep waters (Frank et al., 2003). Such unradiogenic deep water ε_{Nd} at the ROM46 site, more than 1,000 km from land, prompted the authors to invoke additional sources of Nd including Saharan dust and also the Amazon River (Frank et al., 2003). Our new data from Ceara Rise support a far-reaching Amazon source for deep water Nd at the ROM46 site during the Oligocene–Miocene, given that this more distal central Atlantic site yields deep water ε_{Nd} values that fall between those observed at Ceara Rise and contemporaneous northern/southern component water.

4.4. Potential impact of regional terrestrial inputs on seawater ε_{Nd} in the Neogene Ocean

The highly unradiogenic ε_{Nd} composition of suspended particulate material in the Amazon River during the OMT points to more restricted drainage than in the Amazon Basin today, with the dominant terrestrial input coming from the ancient terrane of the Guiana Shield in the East Amazon Basin. The fingerprint of this highly unradiogenic sediment source on deep water ε_{Nd} is recognisable far from the Amazon outflow source, yielding values outside of the range defined by mixing of northern and southern component water masses in the Atlantic. This result is consistent with the findings of Abbott et al. (2015a), who suggest that seawater ε_{Nd} can be strongly affected by inputs of pore fluid Nd if the ε_{Nd} of those pore fluids is significantly offset from that of the overlying water mass.

In more recent geological times the flux and ε_{Nd} composition of the open deep Equatorial Atlantic water mass and Amazon weathering sources have changed. First, the sediment flux from the Amazon increased from the late Miocene to the Pliocene in conjunction with Andean uplift (Figueiredo et al., 2009). This uplift has also resulted in a larger modern Amazon drainage basin that now includes younger Phanerozoic sedimentary rocks (Figueiredo et al., 2009). As the ε_{Nd} of suspended sediments is strongly influenced by drainage pattern changes in the heterogeneous Amazon basin, broadening of the Amazon catchment westwards introduces suspended sediments with more radiogenic compositions ($\varepsilon_{Nd} \sim -10$; Fig. 3A; Allègre et al., 1996; Rousseau et al., 2015). Second, the ε_{Nd} composition of northern component deep water became less radiogenic, starting at about 4 to 3 Ma in the late Neogene (Burton et al., 1997), and is now approximately −13.5 (Piepgras and Wasserburg, 1987). Both of these changes are in a direction that makes it more difficult to discern the influence of regional terrestrial sources from changes in northern/southern component water mass mixing despite the higher Amazon sediment fluxes. For example, a 60% contribution of Nd sourced from the Amazon detrital sediments to Ceara Rise today ($\varepsilon_{Nd} = -10$; Allègre et al., 1996) would be enough to increase the seawater value by 2 ε units above the modern northern component water value. Such a change could be incorrectly interpreted to represent an increased contribution from southern sourced deep waters at this site.

Authigenic ε_{Nd} records for the last 25 thousand years from piston cores GEO B1515-1 and GEOB 1523-1 on Ceara Rise (Fig. 1) show a much more radiogenic signal than we measure across the OMT, with values changing from about −10 at the last glacial maximum to approximately −12 or −13 for the Holocene (Lippold et al., 2016). This Pleistocene to Holocene shift is interpreted to be the result of a change in water mass provenance at Ceara Rise, from predominantly Atlantic southern component water to more unradiogenic northern component water (Lippold et al., 2016). The Holocene Nd isotope compositions in these cores match modern seawater ε_{Nd} (Piepgras and Wasserburg, 1987). We note however that these (de-)glacial deep water ε_{Nd} values are close to modern Amazon suspended sediment values. Therefore, a potential alternative explanation for these Pleistocene ε_{Nd} data could be a greater influence of the benthic sedimentary flux of Nd (∼60% of total Nd) on deep water at Ceara Rise during the last glacial maximum. This could be due to increased exposure time to the benthic sedimentary Nd flux (e.g. Abbott et al., 2015a) during this time of more sluggish Atlantic oceanic overturning (Lippold et al., 2016). Yet because both an increased contribution of southern component water, and a higher flux of benthic (pore fluid) Nd, act to shift deep water ε_{Nd} towards more radiogenic values, the effect of enhanced Nd release from the particulate fraction at the last glacial maximum at Ceara Rise cannot be unambiguously resolved at this stage.

5. Conclusions

We present ε_{Nd} records in fossilised fish teeth, planktonic foraminifera and Fe–Mn oxyhydroxide substrates from Ceara Rise for the Oligocene–Miocene transition. Records from these three substrates are remarkably consistent with one another, implying that all three archives have acquired the ε_{Nd} signature of bottom waters. Yet the ε_{Nd} data that we have obtained are extremely unradiogenic (down to −15) in comparison to those for contemporaneous bottom waters in the Atlantic Ocean. They cannot therefore be explained by simple large-scale ocean mixing between northern and southern component Atlantic deep waters, both of which were significantly more radiogenic (ε_{Nd} of −10 and −8 respectively). We suggest that bottom waters at Ceara Rise were strongly influenced by inputs of Nd derived from weathering of ancient cratonic rocks in the eastern Amazon drainage basin. The similarity between the fish teeth, planktonic foraminifera, and Fe–Mn oxyhydroxide Nd isotope records provides evidence for significant release of Nd from sedimentary particulate material from the River Amazon during the OMT. Discovery of such a strong regional continental influence on deep waters, many hundreds of kilometres from source, suggests that boundary exchange processes can operate far from continental shelf regions (under high particle flux conditions). Caution must therefore be exercised in site selection and when interpreting seawater ε_{Nd} records in light of the vast distances across which major point sources of Nd may influence deep water ε_{Nd}. On the other hand, these techniques present an opportunity to investigate changes in sourcing of riverine-supplied Nd to the ocean associated with major tectonic and/or climatic change.

Acknowledgements

This work used samples provided by the (Integrated) Ocean Drilling Program (ODP), which is sponsored by the US National Science Foundation and participating countries under management of the Joint Oceanographic Institutions (JOI), Inc. We thank Walter Hale and staff at the Bremen Core Repository for their help in obtaining core material and also Guy Rothwell of BOSCORF for providing core top material for production of our in-house foraminiferal calcite standards. We thank Dieter Garbe-Schönberg (University Kiel) and Ana Kolevica (GEOMAR Kiel) for their help in detrital sample processing. We are indebted to Gavin Foster, Carrie Lear, Dan Murphy, Fred Le Moigne, Helen Griffin and Anya Crocker for their advice and helpful discussion of the manuscript. We also thank Derek Vance for assistance with deconvolution of Nd isotope data and Matt Cooper, Darryl Green and Andy Milton for their help with laboratory work. Three anonymous reviewers and the editor

provided constructive reviews that improved an earlier version of the manuscript.

Financial support was provided by the UK Natural Environment Research Council, award # NE/D005108/1 to R.H.J and NE/K014137/1 and a Royal Society Research Merit Award to P.A.W.

Appendix A. Supplementary material

Supplementary material related to this article can be found online at http://dx.doi.org/10.1016/j.epsl.2016.08.037.

References

Abbott, A.N., Haley, B.A., McManus, J., 2015a. Bottoms up: sedimentary control of the deep North Pacific Ocean's ε_{Nd} signature. Geology 43, 1035.

Abbott, A.N., Haley, B.A., McManus, J., Reimers, C.E., 2015b. The sedimentary flux of dissolved rare earth elements to the ocean. Geochim. Cosmochim. Acta 154, 186–200.

Allègre, C.J., Dupré, B., Négrel, P., Gaillardet, J., 1996. Sr–Nd–Pb isotope systematics in Amazon and Congo River systems: constraints about erosion processes. Chem. Geol. 131, 93–112.

Arbuszewski, J.A., deMenocal, P.B., Cleroux, C., Bradtmiller, L., Mix, A., 2013. Meridional shifts of the Atlantic intertropical convergence zone since the Last Glacial Maximum. Nat. Geosci. 6, 959–962.

Arsouze, T., Dutay, J.C., Lacan, F., Jeandel, C., 2009. Reconstructing the Nd oceanic cycle using a coupled dynamical – biogeochemical model. Biogeosciences 6, 2829–2846.

Bayon, G., German, C.R., Burton, K.W., Nesbitt, R.W., Rogers, N., 2004. Sedimentary Fe–Mn oxyhydroxides as paleoceanographic archives and the role of aeolian flux in regulating oceanic dissolved REE. Earth Planet. Sci. Lett. 224, 477–492.

Billups, K., Channell, J.E.T., Zachos, J., 2002. Late Oligocene to early Miocene geochronology and paleoceanography from the subantarctic South Atlantic. Paleoceanography 17, 1004.

Blaser, P., Lippold, J., Gutjahr, M., Frank, N., Link, J.M., Frank, M., 2016. Extracting foraminiferal seawater Nd isotope signatures from bulk deep sea sediment by chemical leaching. Chem. Geol. 439, 189–204.

Bohm, E., Lippold, J., Gutkar, M., Frank, M., Blaser, P., Antz, B., Fohlmeister, J., Frank, Andersen, M.B., Deininger, M., 2015. Strong and deep Atlantic meridional overturning circulation during the last glacial cycle. Nature 517, 73–76.

Burton, K.W., Ling, H.-F., O'Nions, R.K., 1997. Closure of the Central American Isthmus and its effect on deep-water formation in the North Atlantic. Nature 386, 382–385.

Campbell, K.E., Frailey, C.D., Romero-Pittman, L., 2006. The Pan-Amazonian Ucayali Peneplain, late Neogene sedimentation in Amazonia, and the birth of the modern Amazon River system. Palaeogeogr. Palaeoclimatol. Palaeoecol. 239, 166–219.

Carter, P., Vance, D., Hillenbrand, C.D., Smith, J.A., Shoosmith, D.R., 2012. The neodymium isotopic composition of waters masses in the eastern Pacific sector of the Southern Ocean. Geochim. Cosmochim. Acta 79, 41–59.

Channell, J.E.T., Galeotti, S., Martin, E.E., Billups, K., Scher, H.D., Stoner, J.S., 2003. Eocene to Miocene magnetostratigraphy, biostratigraphy, and chemostratigraphy at ODP Site 1090 (sub-Antarctic South Atlantic). Geol. Soc. Am. Bull. 115, 607–623.

Cunha, P.R.C., Gonzaga, F.G., Coutinho, L.F.C., Feijó, F.J., 1994. Bacia do Amazonas. Bol. Geoci. Petrobras 8 (1), 47–55.

Dobson, D.M., Dickens, G.R., Rea, D.K., 2001. Terrigenous sediment on Ceara Rise: a Cenozoic record of South American orogeny and erosion. Palaeogeogr. Palaeoclimatol. Palaeoecol. 165, 215–229.

Eiras, J.F., Becker, C.R., Souza, E.M., Gonzaga, F.G., Silva, J.G.F., Daniel, L.M.F., Matsuda, N.S., Feijó, F.J., 1994. Bacia do Solimões. Bol. Geoci. Petrobras 8 (1), 17–22.

Elmore, A.C., Piotrowski, A.M., Wright, J.D., Scrivner, A.E., 2011. Testing the extraction of past seawater Nd isotopic composition from North Atlantic deep sea sediments and foraminifera. Geochem. Geophys. Geosyst. 12, Q09008.

Figueiredo, J., Hoorn, C., van der Ven, P., Soares, E., 2009. Late Miocene onset of the Amazon River and the Amazon deep-sea fan: evidence from the Foz do Amazonas Basin. Geology 37, 619–622.

Frank, M., van de Flierdt, T., Halliday, A.N., Kubik, P.W., Hattendorf, B., Gunther, D., 2003. Evolution of deepwater mixing and weathering inputs in the central Atlantic Ocean over the past 33 Myr. Paleoceanography 18, 1091.

Gibbs, R.J., 1967. The geochemistry of the Amazon River system: part I. The factors that control the salinity and the composition and concentration of the suspended solids. Geol. Soc. Am. Bull. 78, 1203–1232.

Goldstein, S.J., Jacobsen, S.B., 1987. The Nd and Sr isotopic systematics of river-water dissolved material: implications for the sources of Nd and Sr in seawater. Chem. Geol., Isot. Geosci. Sect. 66, 245–272.

Goldstein, S.L., Hemming, S.R., 2003. Long-lived isotopic tracers in oceanography, paleoceanography, and ice-sheet dynamics. Treatise Geochem. 6, 453–489.

Gutjahr, M., Frank, M., Stirling, C.H., Klemm, V., van de Flierdt, T., Halliday, A.N., 2007. Reliable extraction of a deepwater trace metal isotope signal from Fe–Mn oxyhydroxide coatings of marine sediments. Chem. Geol. 242, 351–370.

Jeandel, C., 1993. Concentration and isotopic composition of Nd in the South Atlantic Ocean. Earth Planet. Sci. Lett. 117, 581–591.

Jeandel, C., Arsouze, T., Lacan, F., Téchiné, P., Dutay, J.C., 2007. Isotopic Nd compositions and concentrations of the lithogenic inputs into the ocean: a compilation, with an emphasis on the margins. Chem. Geol. 239, 156–164.

Kraft, S., Frank, M., Hathorne, E.C., Weldeab, S., 2013. Assessment of seawater Nd isotope signatures extracted from foraminiferal shells and authigenic phases of Gulf of Guinea sediments. Geochim. Cosmochim. Acta 121, 414–435.

Lacan, F., Jeandel, C., 2005a. Acquisition of the neodymium isotopic composition of the North Atlantic Deep Water. Geochem. Geophys. Geosyst. 6, Q12008.

Lacan, F., Jeandel, C., 2005b. Neodymium isotopes as a new tool for quantifying exchange fluxes at the continent–ocean interface. Earth Planet. Sci. Lett. 232, 245–257.

Lang, D.C., Bailey, I., Wilson, P.A., Foster, G.L., Gutjahr, M., Chalk, T.B., 2016. Incursions of southern-sourced water into the deep North Atlantic during late Pliocene glacial intensification. Nat. Geosci. 9, 375–379.

Liebrand, D., Beddow, H., Lourens, L., Palike, H., Raffi, I., Bohaty, S.M., Hilgen, F., Saes, M., Wilson, P.A., van Dijk, A., Hodell, D., Kroon, D., Huck, C., Batenburg, S., 2016. Cyclostratigraphy and eccentricity tuning of the early Oligocene through early Miocene (30.1–17.1 Ma): Cibicides mundulus stable oxygen and carbon isotope records from Walvis Ridge Site 1264. Earth Planet. Sci. Lett. 450, 392–405.

Liebrand, D., Lourens, L.J., Hodell, D.A., de Boer, B., van de Wal, R.S.W., Pälike, H., 2011. Antarctic ice sheet and oceanographic response to eccentricity forcing during the early Miocene. Clim. Past 7, 869–880.

Lippold, J., Gutjahr, M., Blaser, P., Christner, E., de Carvalho Ferreira, M.L., Mulitza, S., Christl, M., Wombacher, F., Böhm, E., Antz, B., Cartapanis, O., Vogel, H., Jaccard, S.L., 2016. Deep water provenance and dynamics of the (de)glacial Atlantic meridional overturning circulation. Earth Planet. Sci. Lett. 445, 68–78.

Martin, E.E., Haley, B.A., 2000. Fossil fish teeth as proxies for seawater Sr and Nd isotopes. Geochim. Cosmochim. Acta 64, 835–847.

Martin, E.E., Scher, H.D., 2004. Preservation of seawater Sr and Nd isotopes in fossil fish teeth: bad news and good news. Earth Planet. Sci. Lett. 220, 25–39.

McDaniel, D.K., McLennan, S.M., Hanson, G.N., 1997. Provenance of Amazon Fan muds: constraints from Nd and Pb isotopes. In: Flood, R.D., Piper, D.J.W., Klaus, A., Peterson, L.C. (Eds.), Proceedings of the Ocean Drilling Program, Scientific Results, vol. 155, pp. 169–176.

O'Nions, R.K., Frank, M., von Blanckenburg, F., Ling, H.F., 1998. Secular variation of Nd and Pb isotopes in ferromanganese crusts from the Atlantic, Indian and Pacific Oceans. Earth Planet. Sci. Lett. 155, 15–28.

Osborne, A.H., Haley, B.A., Hathorne, E.C., Flögel, S., Frank, M., 2014. Neodymium isotopes and concentrations in Caribbean seawater: tracing water mass mixing and continental input in a semi-enclosed ocean basin. Earth Planet. Sci. Lett. 406, 174–186.

Pälike, H., Frazier, J., Zachos, J.C., 2006. Extended orbitally forced palaeoclimatic records from the equatorial Atlantic Ceara Rise. Quat. Sci. Rev. 25, 3138–3149.

Pearce, C.R., Jones, M.T., Oelkers, E.H., Pradoux, C., Jeandel, C., 2013. The effect of particulate dissolution on the neodymium (Nd) isotope and Rare Earth Element (REE) composition of seawater. Earth Planet. Sci. Lett. 369–370, 138–147.

Piepgras, D.J., Wasserburg, G.J., 1987. Rare earth element transport in the western North Atlantic inferred from Nd isotopic observations. Geochim. Cosmochim. Acta 51, 1257–1271.

Piotrowski, A.M., Goldstein, S.L., Hemming, S.R., Fairbanks, R.G., 2005. Temporal relationships of carbon cycling and ocean circulation at glacial boundaries. Science 307, 1933–1938.

Pomiès, C., Davies, G.R., Conan, S.M.H., 2002. Neodymium in modern foraminifera from the Indian Ocean: implications for the use of foraminiferal Nd isotope compositions in paleo-oceanography. Earth Planet. Sci. Lett. 203, 1031–1045.

Rempfer, J., Stocker, T.F., Joos, F., Dutay, J.-C., Siddall, M., 2011. Modelling Nd-isotopes with a coarse resolution ocean circulation model: sensitivities to model parameters and source/sink distributions. Geochim. Cosmochim. Acta 75, 5927–5950.

Roberts, N.L., Piotrowski, A.M., Elderfield, H., Eglinton, T.I., Lomas, M.W., 2012. Rare earth element association with foraminifera. Geochim. Cosmochim. Acta 94, 57–71.

Rosenthal, Y., Field, M.P., Sherrell, R.M., 1999. Precise determination of element/calcium ratios in calcareous samples using sector field inductively coupled plasma mass spectrometry. Anal. Chem. 71, 3248–3253.

Rousseau, T.C.C., Sonke, J.E., Chmeleff, J., van Beek, P., Souhaut, M., Boaventura, G., Seyler, P., Jeandel, C., 2015. Rapid neodymium release to marine waters from lithogenic sediments in the Amazon estuary. Nat. Commun. 6.

Scher, H.D., Martin, E.E., 2004. Circulation in the Southern Ocean during the Paleogene inferred from neodymium isotopes. Earth Planet. Sci. Lett. 228, 391–405.

Scher, H.D., Martin, E.E., 2006. Timing and climatic consequences of the opening of drake passage. Science 312, 428–430.

Scher, H.D., Martin, E.E., 2008. Oligocene deep water export from the North Atlantic and the development of the Antarctic Circumpolar Current examined with neodymium isotopes. Paleoceanography 23, PA1205.

Shephard, G.E., Muller, R.D., Liu, L., Gurnis, M., 2010. Miocene drainage reversal of the Amazon River driven by plate–mantle interaction. Nat. Geosci. 3, 870–875.

Shipboard Scientific Party, 1995. Site 926. In: Curry, W.B., Shackleton, N.J., Richter, C., et al. (Eds.), Proceedings of the Ocean Drilling Program. Initial Reports. College Station, TX (Ocean Drilling Program), vol. 154, pp. 153–232.

Stewart, J.A., Wilson, P.A., Edgar, K.M., Anand, P., James, R.H., 2012. Geochemical assessment of the palaeoecology, ontogeny, morphotypic variability and palaeoceanographic utility of "Dentoglobigerina" venezuelana. Mar. Micropaleontol. 84–85, 74–86.

Stichel, T., Frank, M., Rickli, J., Haley, B.A., 2012. The hafnium and neodymium isotope composition of seawater in the Atlantic sector of the Southern Ocean. Earth Planet. Sci. Lett. 317–318, 282–294.

Tachikawa, K., Athias, V., Jeandel, C., 2003. Neodymium budget in the modern ocean and paleo-oceanographic implications. J. Geophys. Res. 108, 3254.

Tachikawa, K., Piotrowski, A.M., Bayon, G., 2014. Neodymium associated with foraminiferal carbonate as a recorder of seawater isotopic signatures. Quat. Sci. Rev. 88, 1–13.

Tanaka, T., Togashi, S., Kamioka, H., Amakawa, H., Kagami, H., Hamamoto, T., Yuhara, M., Orihashi, Y., Yoneda, S., Shimizu, H., Kunimaru, T., Takahashi, K., Yanagi, T., Nakano, T., Fujimaki, H., Shinjo, R., Asahara, Y., Tanimizu, M., Dragusanu, C., 2000. JNdi-1: a neodymium isotopic reference in consistency with LaJolla neodymium. Chem. Geol. 168, 279–281.

Thomas, D.J., Bralower, T.J., Jones, C.E., 2003. Neodymium isotopic reconstruction of late Paleocene–early Eocene thermohaline circulation. Earth Planet. Sci. Lett. 209, 309–322.

van der Hammen, T., Hooghiemstra, H., 2000. Neogene and Quaternary history of vegetation, climate, and plant diversity in Amazonia. Quat. Sci. Rev. 19, 725–742.

Vance, D., Burton, K., 1999. Neodymium isotopes in planktonic foraminifera: a record of the response of continental weathering and ocean circulation rates to climate change. Earth Planet. Sci. Lett. 173, 365–379.

Vance, D., Scrivner, A.E., Beney, P., Staubwasser, M., Henderson, G.M., Slowey, N.C., 2004. The use of foraminifera as a record of the past neodymium isotope composition of seawater. Paleoceanography 19, PA2009.

Vance, D., Thirlwall, M., 2002. An assessment of mass discrimination in MC-ICPMS using Nd isotopes. Chem. Geol. 185, 227–240.

Wang, X., Auler, A.S., Edwards, R.L., Cheng, H., Cristalli, P.S., Smart, P.L., Richards, D.A., Shen, C.-C., 2004. Wet periods in northeastern Brazil over the past 210 kyr linked to distant climate anomalies. Nature 432, 740–743.

West, A.J., Galy, A., Bickle, M., 2005. Tectonic and climatic controls on silicate weathering. Earth Planet. Sci. Lett. 235, 211–228.

Wilson, D.J., Piotrowski, A.M., Galy, A., McCave, I.N., 2012. A boundary exchange influence on deglacial neodymium isotope records from the deep western Indian Ocean. Earth Planet. Sci. Lett. 341–344, 35–47.

Wombacher, F., Rehkämper, M., 2003. Investigation of the mass discrimination of multiple collector ICP-MS using neodymium isotopes and the generalised power law. J. Anal. At. Spectrom. 18.